ELSEVIER

Biophysical Chemistry 100 (2003) 281–292

Biophysical Chemistry

www.elsevier.com/locate/bpc

Modeling of electrostatic recognition processes in the mammalian mitochondrial steroid hydroxylase system

Jürgen J. Müller[a,*], Anna Lapko[a,1], Klaus Ruckpaul[a], Udo Heinemann[a,b]

[a]*Max-Delbrück-Centrum für Molekulare Medizin Berlin-Buch, Robert-Rössle-Str. 10, D-13125 Berlin, Germany*
[b]*Institut für Chemie/Kristallographie, Freie Universität Berlin, Takustr. 6, D-14195 Berlin, Germany*

Received 13 February 2002; accepted 3 May 2002

Abstract

Adrenodoxin reductase (AR) and adrenodoxin (Adx) are components of the mammalian mitochondrial steroid-hydroxylating system. Crystal structures of Adx, AR and a cross-linked Adx–AR complex have recently been determined. Based on these, we have carried out a modeling and docking study to characterize the recognition between AR, Adx and cytochrome *c* (Cyt*c*). To rationalize the recognition process, electrostatic potentials were calculated by solving the Poisson–Boltzmann equations. In the Adx–AR complex modeled, a negatively charged surface of Adx recognizes a positive surface of AR, as in the crystal structure of the Adx–AR complex, proving the correct parameterization for the energy calculations. After forming salt bridges between the polar primary binding sites of Adx and AR, charge compensation causes a domain movement in AR, which closes the binding cleft by 2–4 Å. Thereby, a secondary polar binding site is closed and the electron transfer pathways between the FAD of AR and the [2Fe–2S] cluster of Adx are adjusted. Next, the model structure of a complex between Adx and Cyt*c* was derived. The lowest-energy complex between Adx and Cyt*c* matches earlier chemical modification and cross-linking experiments, which proposed polar interactions of Lys13, Lys27, Lys72 and Lys79 of Cyt*c* with acidic residues in Adx. Because of the short distance of 9.4 Å between the redox centers, a complex, productive in electron transfer via a different outlet pathway from the inlet route in Adx, is expected. However, a ternary complex cannot be formed between the Adx–AR complex and Cyt*c* because of steric hindrance. Therefore, a shuttle model for the role of Adx in the electron transfer process to Cyt*c* is preferable to a relay model. In addition, no preferable docking site could be detected for a second Adx when probing the Adx–AR complex, which is required for a quaternary organized-cluster model of all redox partners of the hydroxylase system.

Keywords: Adrenodoxin; Adrenodoxin reductase; Cytochrome *c*; Modeling of complex building; Electrostatic recognition

*Corresponding author. Tel.: +49-30-9406-3421; fax: +49-30-9406-2548.
E-mail addresses: jjm@mdc-berlin.de (J.J. Müller), heinemann@mdc-berlin.de (U. Heinemann).
[1] On leave from the International Sakharow Institute of Radioecology, 2220009 Minsk, Belarus.

0301-4622/03/$ - see front matter
PII: S0301-4622(02)00286-7

1. Introduction

The mammalian mitochondrial steroid hydroxylating system of the adrenal gland consists of three macromolecular components, a nicotinamide adenine dinucleotide phosphate [NADP(H)]-dependent adrenodoxin reductase (AR), the [2Fe–2S] cluster-containing adrenodoxin (Adx), and a catalytically active cytochrome P450 (P450scc). The conversion of steroids during hormone biosynthesis requires electrons, which are transported from AR to P450 by Adx sequentially. The three-dimensional structures of Adx [1], AR [2,3] and of a covalently cross-linked complex of both [4] have recently been solved, providing insight into the structural basis of the electron transfer reaction.

Numerous biochemical experiments, including chemical modification [5,6], site-specific mutations [7–9] and chemical cross-linking [10–12], have been performed to characterize interactions and electron transfer pathways within the hydroxylase system. Complex formation is predominantly driven through electrostatic forces, but hydrophobic patches also play a role during the interaction. The soluble cytochrome *c* (Cyt*c*) is frequently used in Adx–Cyt*c* or AR–Adx–Cyt*c* assays as a final, spectroscopically active electron receptor in place of the membrane-attached P450 when the aim is to characterize the electron transfer efficiency of the system in vitro. Adx reduces Cyt*c* in vitro, but the reaction is probably not of physiological relevance, since the two proteins are located at opposite sides of the inner mitochondrial membrane of the adrenal cortex [13]. At low ionic strength they form stable complexes with a dissociation constant of 34 nM [14]. Intermolecular interactions in the 1:1 complex are mainly ionic in character [15]. Up to now, no systematic screening for residues of Cyt*c* interacting with components of the hydroxylase system has been undertaken. However, changes in the interactions with Cyt*c* in the electron transfer assays could influence the results attributed to the hydroxylase system components. It is well known that reduced Adx reacts extremely rapidly to reduce Cyt*c* in complex with AR, as well as without the reductase [16]. Therefore, there are several points of interest to be investigated. Firstly, which residues belong to the binding sites, and secondly, does Cyt*c* bind to Adx in a unique way, or do different binding sites for Cyt*c* exist in Adx free in solution or when complexed with AR?

We are primarily interested in the role of Adx in electron transfer from AR to P450. Up to now, two different models have been considered: the organized cluster models [17,18], as opposed to the shuttle model [16], where Adx sequentially transports one electron after the other from AR to P450scc. These models may be probed by analyzing the electron transport from the [2Fe–2S] cluster to the Adx surface. In organized cluster models where one or two Adx molecules function as relays for the electron transport between AR and P450, alternative electron transfer pathways are expected to exist. If, conversely, a shuttle model is valid, identical pathways within Adx may, in principle, be used for electron transport from AR and to P450. Here, we used Cyt*c* and Adx as probes to search for a secondary donor–acceptor pathway from the [2Fe–2S] cluster to the Adx surface.

To address the above issues, we set out to derive model structures of binary or ternary complexes involving Adx, AR and Cyt*c*, making use of the available crystal structures of all proteins and of experimental data such as cross-links and chemical modifications at the protein surfaces. Using these restraints permits establishment of theoretical models of biological relevance. To prove that the docking calculations were parameterized with suitable energy terms, we started with electrostatic and van der Waals energy-minimization calculations for the known complex of Adx–AR. Subsequent modeling of the docking of Adx to uncomplexed AR provided some insight into the recognition process yielding the Adx–AR complex. Finally, we modeled the docking of Cyt*c* to Adx and to the covalent Adx–AR complex, and probed the Adx–AR complex with a secondary Adx. The results support the shuttle hypothesis for Adx.

2. Materials and methods

2.1. Data preparation

The crystal structure of truncated bovine Adx [Adx(4–108)], lacking the N-terminal residues

Ser1–Glu4 and the C-terminus from Asp109 to Glu128 of Adx, was recently determined [1] [Protein Data Bank (PBD) entry 1AYF]. The coordinates of the covalently cross-linked complex of wild-type Adx with the adrenodoxin reductase Adx–AR [4] (entry 1E6E), of uncomplexed AR [2] (entry 1CJC), of AR complexed with $NADP^+$ [3] (entry 1E1L), and of horse heart cytochrome *c* [19] (entry 1HRC) were taken from the Protein Databank [20]. The program UHBD [21] was used for calculation of electrostatic potentials, and protein–ligand docking was carried out with DOT [22]. To use these programs, atomic coordinates were prepared as follows. Polar hydrogens were added with CNS [23]. Partial atomic charges for the proteins, heme group, [2Fe–2S] cluster and flavin adenine dinucleotide (FAD) were based on the AMBER library [24]. Histidine side chains were neutral, with one hydrogen either on N^{ε} or N^{δ}, depending on the ligation by Fe or hydrogen bonding. The N-terminus of the acetylated Cyt*c* was neutral and the C-terminus negatively charged. The overall charge of the heme group is -2.4. In Adx the charged residues Glu4, Asp119, Lys126, Glu128, the N-terminus and the flexible C-terminus are not localized in the X-ray structure, and the coordinates of the N-terminus of AR are not known. Because the truncated Adx(4–108) binds to AR, P450scc and Cyt*c* with similar affinity as the wild-type protein, these residues are not expected to play an essential role in recognition and binding processes. To check the parameterization of the system, an initial docking experiment was performed with the aim of reproducing the known Adx–AR complex.

2.2. Electrostatic potentials

Electrostatic potentials were calculated by solving the Poisson–Boltzmann equations with the program UHBD [21]. The grid for the potential values was restricted to maximum dimensions of $128\times128\times128$ Å^3 with 1-Å spacing because of the limits imposed by the docking program DOT [22]. Dielectric constants $\varepsilon=3$ for the protein and $\varepsilon=80$ for the aqueous surrounding, and an ion exclusion radius of 1.4 Å were chosen following the example recently set for the similar system of cytochrome *c* and cytochrome *c* oxidase [25]. From experimental data, an ionic strength of 50–100 mM is suggested for stable Adx–AR [11] and Cyt*c*–Adx [26] complexes.

2.3. Docking experiments

In a series of docking experiments, Adx was first docked on uncomplexed AR [2], mimicking the pre-complex in situ, and then Adx was docked on AR using the coordinates of Adx and AR from the covalently cross-linked Adx–AR complex [4]. Next, Cyt*c* was docked on the cross-linked Adx–AR complex, Cyt*c* was docked on Adx, and finally Adx was docked on the cross-linked Adx–AR complex. The first-mentioned molecule in each computer experiment was allowed to move, and the second was kept stationary, fixed at the origin of the grid. The shape of the moving molecule was approximated by its atomic coordinates and not by the van der Waals volume [22] to permit an approach within 1.5 Å of the stationary molecule and small side-chain conformational changes upon docking. The partial charges were taken from the AMBER library and placed at the atomic positions of the non-hydrogen and polar hydrogen atoms. The shape of the stationary molecule was represented by a 3.0-Å layer of favorable potential. To map the shape potential of the stationary molecule onto the grid, grid points within 4.5 Å of non-hydrogen atoms were assigned a value -1, and then grid points within 1.5 Å of non-hydrogen atoms were assigned a highly unfavorable value of 1000. All other grid points were assigned a value of 0. Large changes in magnitude and distribution of the electrostatic potential were avoided by limiting extreme potentials to $+4$ and -6 kcal mol^{-1} e^{-1} to obtain only a small number of false favorable-energy positions in DOT [25]. In the minimum energy search by DOT, $128\times128\times128$ grid points and 54 000 rotational orientations ($\sim6^\circ$ sampling) were used because of the limitations of DOT. The computational time was 48 h using a heterogeneous network of 8 SGI R12000, R10000, R4400 processors and one 1-GHz Linux-PC in parallel.

3. Results and discussion

3.1. Electrostatic recognition of AR by Adx

The recognition process and complex formation between Adx and AR are strongly ionic strength-dependent [16], and the driving force of the first recognition steps is clearly of electrostatic type. More than 65% of the buried surface in the Adx–AR complex [4] are of polar/polar or of mixed type (Table 1). Each of the molecules has an asymmetric potential caused by the negative charges on Adx and the positive charges on AR (Fig. 1). Both molecules possess strong dipoles in coplanar orientation (not shown). Both partner proteins search for each other in a semi-closed sphere, and subsequently optimize charge and non-polar interactions. Because the crystal structure of uncomplexed AR [2] is used for docking, Adx does not find the same position on AR as in the experimentally determined complex [4]. This result was to be expected, since DOT cannot take into account the induced domain movement that is observed to occur upon complex formation [4]. Despite the rigid AR, the primary binding site of Adx (Asp72, Asp76, Asp79) docks to the primary interaction region of AR (Arg211, Arg240, Arg244) with a maximal offset of 3.5 Å within a plane containing the primary and secondary binding sites of AR (Fig. 1), and of approximately ± 3.5 Å perpendicular to that plane. The secondary binding sites of both molecules (Asp39 and Asp41 in Adx; His28 and Lys27 in AR) are too far from each other to form a salt bridge between Adx Asp39 and AR Lys27, as observed in the Adx–AR crystal structure.

The primary docking event may thus induce the domain motion by charge compensation (Fig. 2), and thereby enable the secondary interaction. This is confirmed by modeling the docking between both components, taking their coordinates from the covalently cross-linked complex [4]. In forming this complex, AR permits a much more precise positioning of Adx in its positively charged cleft (Fig. 2). The 20 lowest-energy configurations found by DOT show a tight clustering of Adx, visualized by the [2Fe–2S] cluster in Fig. 2, in front of the electron donor, the isoalloxazine ring of AR, varying the position nearly coplanar (± 0.5 Å in horizontal directions) within 3 Å. In part, these deviations may be attributed to the grid space of 1 Å, the smallest value possible. The correctness in positioning the movable molecule is obvious upon comparison with the experimental Adx–AR complex, where the third interaction region consists of the peptides Ala45–Thr54 of Adx, and Glu57–Thr64 and Ile376–Met380 of AR, and it is taken as proof of the suitable parameterization needed for the energy calculations.

Table 1
Interface characterization and electron transfer properties of crystallographically analyzed ferredoxin–ferredoxin reductase complexes, of a cytochrome *c*–cytochrome *c* peroxidase complex, and of an Adx–Cyt*c* model complex

Complex	Donor–acceptor distance (Å)	Interaction area (Å^2)				Coupling constant	Experimental electron transfer rate (s^{-1})
		Total	Polar	Hydrophobic	Mixed		
Adx–AR	10.3	2369	508	780	1082	1.7×10^{-6}	3–4
Fd–FNR, *Anabaena*	6.7	1711	431	524	809	3.2×10^{-3}	6000
Fd–FNR, maize leaf	5.9	1771	463	499	846	3.3×10^{-3}	120
Adx–Cyt*c*, model	9.4	1569	246	584	894	7.3×10^{-4}	400
Cyt*c*-peroxidase–Cyt*c*	19.0	1064	265	327	473	7.2×10 [9a]	700–3500

The interaction areas were determined with the program XSAE (C. Broger, personal communication) corresponding to the definition given in [27]. The coupling constant was calculated with the program HARLEM [28]. The crystal structures of bovine Adx–AR, Fd–FNR from *Anabaena*, Fd–FNR from maize leaf and horse cytochrome *c*–cytochrome *c* peroxidase from yeast were recently determined [4,29–31].

[a] Electron transfer pathway differs from the Ala194–Ala193–Gly192–Trp191 peptide proposed by Pelletier and Kraut [31].

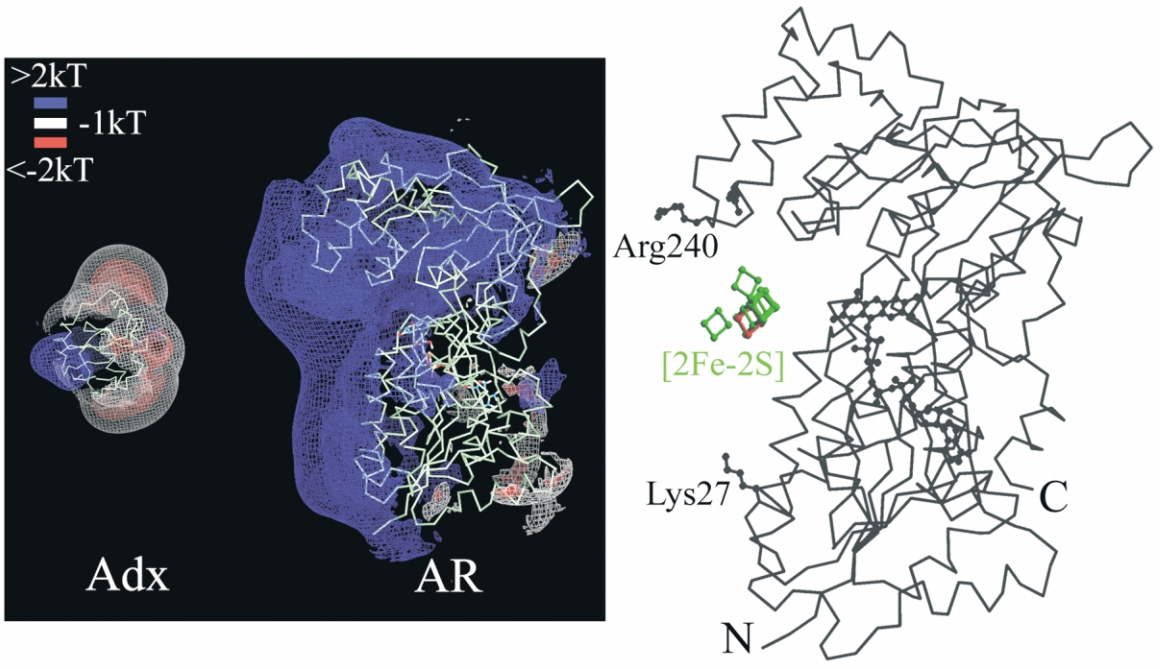

Fig. 1. Molecular modeling of an Adx–AR complex. (a) Electrostatic potentials of Adx and AR calculated with the program UHBD [21]. Blue contours indicate positive and red contours negative potential. AR coordinates are taken from uncomplexed reductase [2]. Adx and AR are oriented as in the modeled complex, but have been shifted apart to reveal the complete potential surfaces. (b) 20 minimum-energy positions of Adx, marked by their [2Fe–2S] cluster position (*green*), and the position of Adx (*red*) within the covalently cross-linked Adx–AR complex [4]. Figures were produced with QUANTA (Molecular Simulations Inc, 1997) and SETOR [32].

Adx binds to AR, independent of the presence of NADPH in the latter. Fig. 3 depicts the electrostatic potential at the Adx–AR complex, which is rotated by 180° with respect to Fig. 2. The positive potential maximum is located within a cleft open for NADPH to diffuse into, resulting in a juxtaposition of its nicotinamide moiety against the isoalloxazine ring of FAD [3]. Either Adx or NADPH induces similar conformational changes upon binding to AR (Fig. 4), exploiting the flexibility of the hinge region between the protein's FAD and NADP domains. The induced distance differences in C^{α}-atom positions between the AR–$NADP^{+}$ [3] and Adx–AR [4] complexes in comparison with uncomplexed AR [2] are comparable. This means that the primary docking of Adx to the AR binding pocket may be facilitated (because the pocket is bigger and more open) if no NADPH is bound to AR. Conversely, Adx binding to the pre-formatted redox partner AR may immediately lead to a tighter complex, followed only by fine tuning of the structure. On the other hand, the diffusion of NADPH into the cleft is somewhat restricted by Adx, acting as a shutter at one of three open sides and by the slight closure of the cleft. To probe the shuttle model for Adx, the sequence of docking events in which NADPH-binding with induced cleft closing is followed by Adx binding, or vice versa, has to be investigated.

3.2. Electrostatic recognition of Adx–AR by Cytc

The Adx–AR complex is less stable ($k_{off}=300$ s^{-1} [16]) than a typical protein–protein, e.g. an inhibitor–protease complex [27]. This is also true for the two other known ferredoxin–ferredoxin reductase complexes from the cyanobacterium *Anabaena* [29] and maize leaf [30,33], as well as

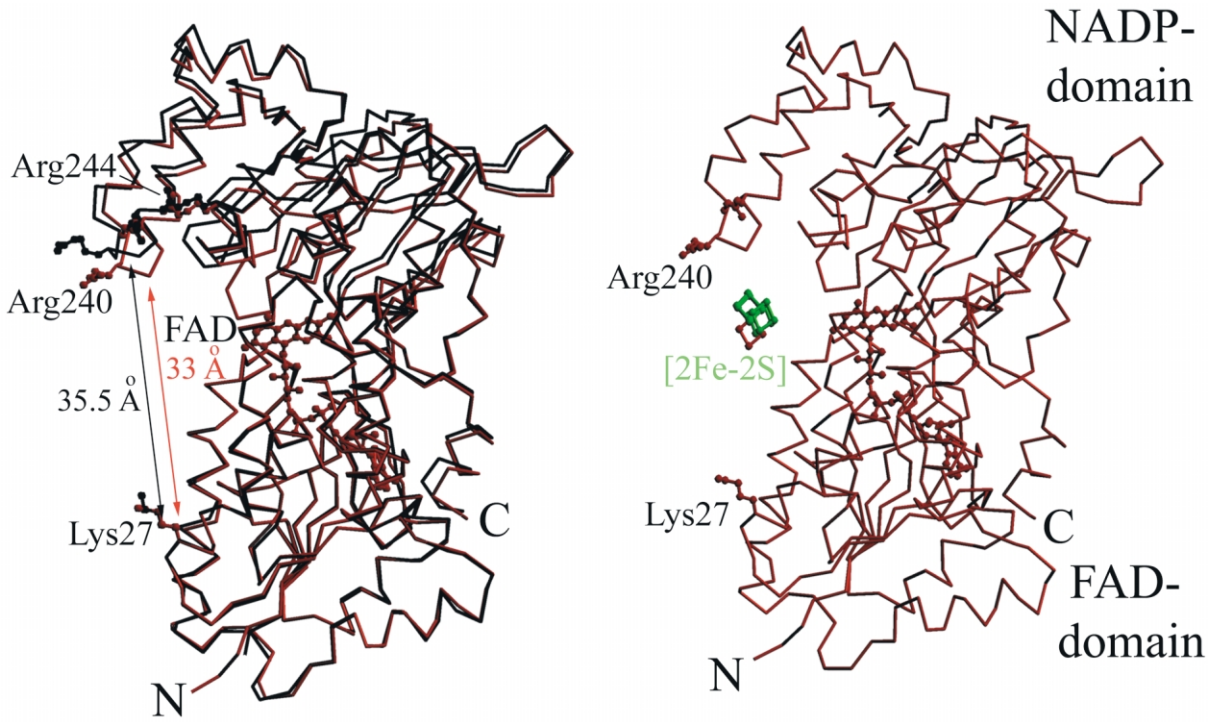

Fig. 2. Induced fit of AR during Adx–AR complex formation. (a) Superposition of the FAD domains of free AR (*black*) and AR from the Adx–AR complex (*red*) shows the domain rearrangement of AR yielding an AR conformation active in electron transfer. (b) 20 minimum-energy positions of Adx, marked by their [2Fe–2S] cluster positions (*green*), docked to active AR (*red*). The [2Fe–2S] cluster in the cross-linked Adx–AR complex is colored red. Figures were produced with SETOR [32].

for the crystallographically characterized complex of cytochrome *c*–cytochrome *c* peroxidase [31], judging from the buried areas within the complexes (Table 1). At least for the ferredoxin–reductase complexes, it is unclear whether the ferredoxin acts like a shuttle, transferring the electrons from one redox partner to the other, or rather like a relay in an organized cluster of all components. In an organized cluster, Adx needs two different pathways for electrons, although overlapping binding sites exist with AR and P450scc [7]: the proposed primary pathway from the isoalloxazine ring of AR to the [2Fe–2S] cluster of Adx [4], and a hypothetical secondary pathway, where the electron moves from the iron–sulfur cluster to the terminal acceptor. To find this outlet we used Cyt*c*, as well as Adx, as a probe for the crystallographic Adx–AR complex. The potential energy distribution around the complex and around Cyt*c* is shown in Fig. 5. Because the region with positive potential around Cyt*c* will interact with the areas of the complex showing residual negative potential, there are only few favorable positions available at the complex surface. The two out of the top 20 configurations of the minimum-energy grid (marked I and II in Fig. 5b), which are near the Adx–AR boundary, are probably not active in electron transfer, because the heme is tangential to the Adx surface and its center is 21–28 Å away from the [2Fe–2S] cluster. The Cyt*c* positions III and IV at the distant AR surface are also non-productive.

3.3. Electrostatic recognition of Adx by Cytc

The crystallized Adx–AR complex [4] is cross-linked between Adx Asp39 and AR Lys27, but the primary interaction region remains freely dis-

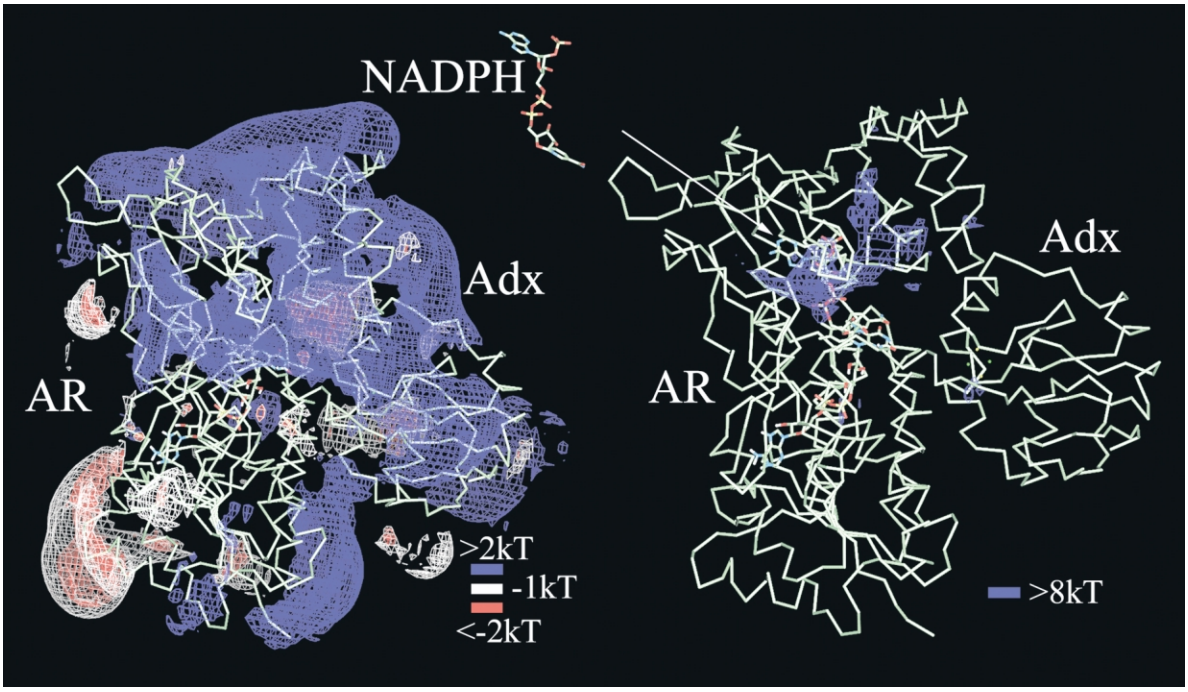

Fig. 3. Electrostatic potential for Adx–AR–NADPH complex formation. (a) Electrostatic potentials of Adx–AR calculated with the program UHBD [21]. AR is rotated by approximately 180° in comparison to Fig. 1. Blue contours indicate positive, red contours negative potential. (b) Electrostatic potential contoured at a higher level. Maximal residual positive-potential is around the binding pocket of NADPH. $NADP^+$ is modeled and positioned within the Adx–AR complex corresponding to [3]. Figures were produced with QUANTA (Molecular Simulations Inc, 1997).

sociable after reduction of Adx. The binding of P450scc to the Adx–AR complex and the activity of the system in transformation of cholesterol to pregnenolone have recently been demonstrated and discussed as strong evidence for such dissociation during electron transfer, thus favoring the shuttle concept [12].

To provide further support for this view, we performed docking experiments between isolated Adx and Cyt*c*. The top 20 configurations of the minimum-energy grid and the most probable active Cyt*c*–Adx complex with the lowest energy are shown in Fig. 6a. The interaction map of the minimum-energy complex (Fig. 7) shows four regions of Adx, Ile25–Asp31, Cys46–Leu50, Glu68–Glu73 and Cys92–Thr97, to be in contact with the Cyt*c* peptides Val11–Cys17, Lys27–Thr28 and Asn70–Lys86. These Cyt*c* peptides contain lysines Lys13, Lys27, Lys72, Lys79, all suggested by chemical probing [5] as candidates for interaction sites with Adx, as well as with cytochrome *c* oxidase [35], and several of the lysines (Lys13, Lys72, Lys86) detected in the interaction site of the crystallographically characterized Cyt*c*–cytochrome *c* peroxidase complex [31]. In particular, the Cyt*c* residue Lys13 is attached to the Adx peptide Glu68–Glu73, which was found earlier by cross-linking experiments [34]. The Adx residues Glu74, Asp79 and Asp86 are not located within the interface, and their modification would not influence the interaction with Cyt*c* as found earlier, too [36].

The buried area between Cyt*c* and Adx is similar to the ferredoxin interaction areas of the known electron-transfer complexes as given in Table 1, and the Cyt*c*–Adx complex tends to be less stable than the Adx–AR complex. Of course, the interaction areas for the modeled Cyt*c*–Adx complex

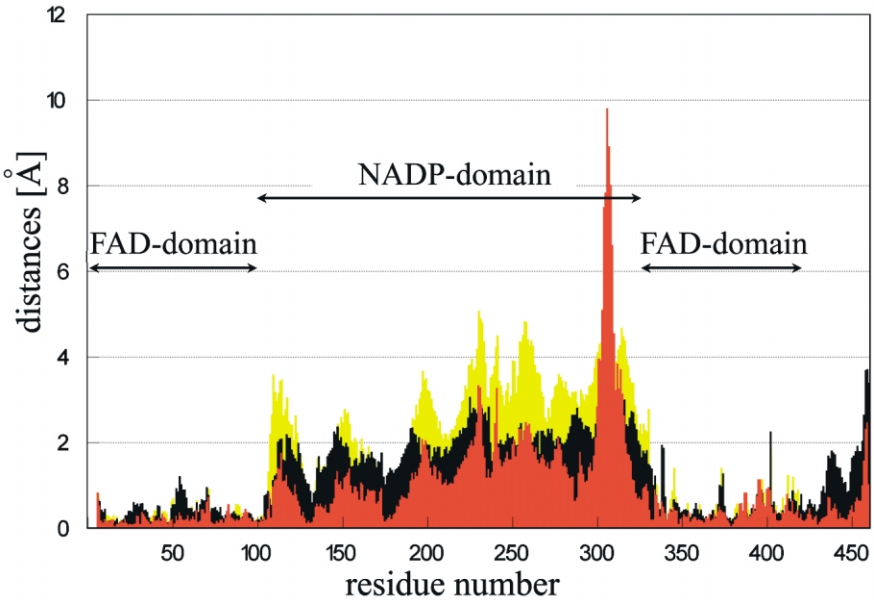

Fig. 4. Distances between C^{α} atoms of free and complexed AR molecules. After superposition of the FAD domains, the distances between C^{α} atoms of free AR, AR in the cross-linked complex (red, molecule A; yellow, molecule B), and AR co-crystallized with $NADP^{+}$ (colored black) [3] show the equivalence of AR domain movement caused by Adx or $NADP^{+}$ binding.

can only be approximate, because DOT is not capable of changing side-chain conformations, which is possibly required for optimal interaction. Since Adx should not need to dissociate from the Adx–AR complex during electron transfer from NADPH to Cyt*c* [37], after formation of the Cyt*c*–Adx complex, it was tried to fit this complex to AR in a way that reproduces the Adx–AR recognition observed within the Adx–AR complex [4]. It is observed that steric hindrance by AR will prevent formation of this type of ternary complex between Adx, AR and Cyt*c*. However, after a slight movement of the Adx component by approximately 2–5 Å from the AR surface, the Cyt*c*–Adx complex described can be established. This is in agreement with the inactivity of the cross-linked Cyt*c*–Adx towards AR [34], because the Cyt*c*–Adx complex can only be formed with reduced Adx after dissociation from AR.

The acetate group at the N-terminus of Cyt*c* is in direct contact with AR, which may have disturbed complex formation in earlier experiments [6]. Unfortunately, the model does not explain the higher binding constant to Cyt*c* for the wild-type Adx in comparison to the truncated form, because the C-terminus of Adx is opposite to the Cyt*c*-docking site.

Most probably, between Adx and Cyt*c*, the electron uses a recently proposed secondary pathway along Adx Fe2/Cys92 rather than Fe1/Cys52 [38]. The distance between the donor and acceptor edge is approximately 9.4 Å and the theoretical coupling constant (Table 1) is higher than between Adx and AR, in agreement with the experimental electron-transfer rate of 400 s^{-1} [16]. The rate-limiting step of the electron transfer from AR to Cyt*c* should be between Adx and AR, in agreement with the experimental results [39]. Although we assume a secondary electron pathway in Adx, different from the primary one, the small molecule Cyt*c* may also be reduced by a shuttle rather than by a relay mechanism. This is also possible in a cytochrome reduction assay when Adx is covalently cross-linked to AR [11]. Fig. 6b shows a possible arrangement of the ternary complex, where Adx rotates around the cross-linked residues

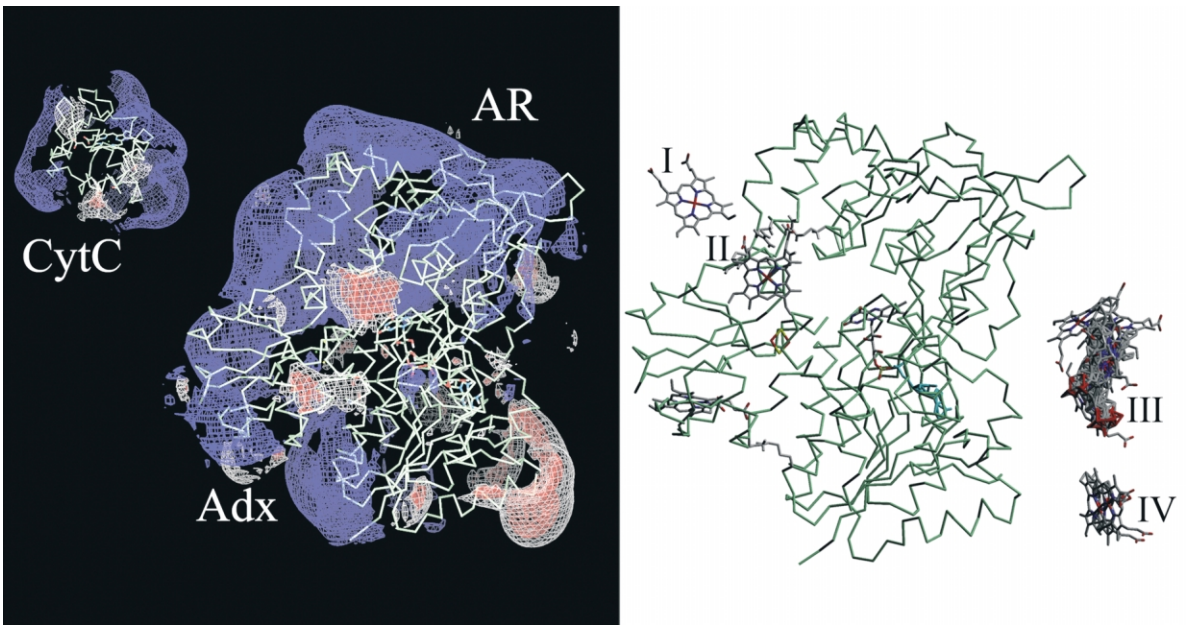

Fig. 5. Docking of Cyt*c* to Adx–AR. (a) Electrostatic potentials of Cyt*c* and Adx–AR calculated with the program UHBD [21]. The blue contours indicate positive, red contours negative potential. Cyt*c* coordinates were taken from PDB entry 1HRC [19]. (b) 20 minimum-energy positions of Cyt*c* marked by their hemes (stick presentation) around the covalently cross-linked complex (green C^{α} trace) [4]. Figures were produced with QUANTA (Molecular Simulations Inc, 1997) and SETOR [32].

Adx-Asp39 and AR-Lys27. Normally, Adx would move from AR to Cyt*c* without being tethered by the cross-link.

3.4. Electrostatic recognition of Adx by Adx

Recently, quaternary complexes of AR–$(Adx)_2$–P450scc have been discussed [18]. To explore this possibility, we used Adx as a probe on the Adx–AR complex in a further set of docking experiments. Because the most prominent residual positive potential is located at the NADPH cleft site of the Adx–AR complex (Fig. 3), the second Adx will dock at the NADP domain of AR and/or near the boundary between AR and the primary Adx. For the most energetically favorable complexes resulting from docking, the [2Fe–2S] cluster and Glu79 [12,40] of the second Adx are accessible for P450scc, but the distance between the [2Fe–2S] clusters within the first and the second Adx is unfavorably large for electron transfer (35 Å). Four of the top 20 energetically favorably positioned Adx are in contact with the Adx molecule bound to AR first. Here, the redox centers are 23–25 Å from each other and Glu79 is accessible to P450scc, but the secondary iron–sulfur cluster is buried between the two Adx molecules and not neighbored to the heme group of P450scc. A third group of docked Adx blocks the NADPH binding cleft by its C-terminus. No secondary Adx has been detected in a similar position as predicted from crystal packing [41]. In conclusion, a secondary position for docking of Adx as an anchor for P450scc when assembling an organized complex of all redox partners of the cholesterol hydroxylase system could not be detected using the known structures of the oxidized components.

Acknowledgments

This paper honors the lasting contributions to physical biochemistry of Prof John T. Edsall. We

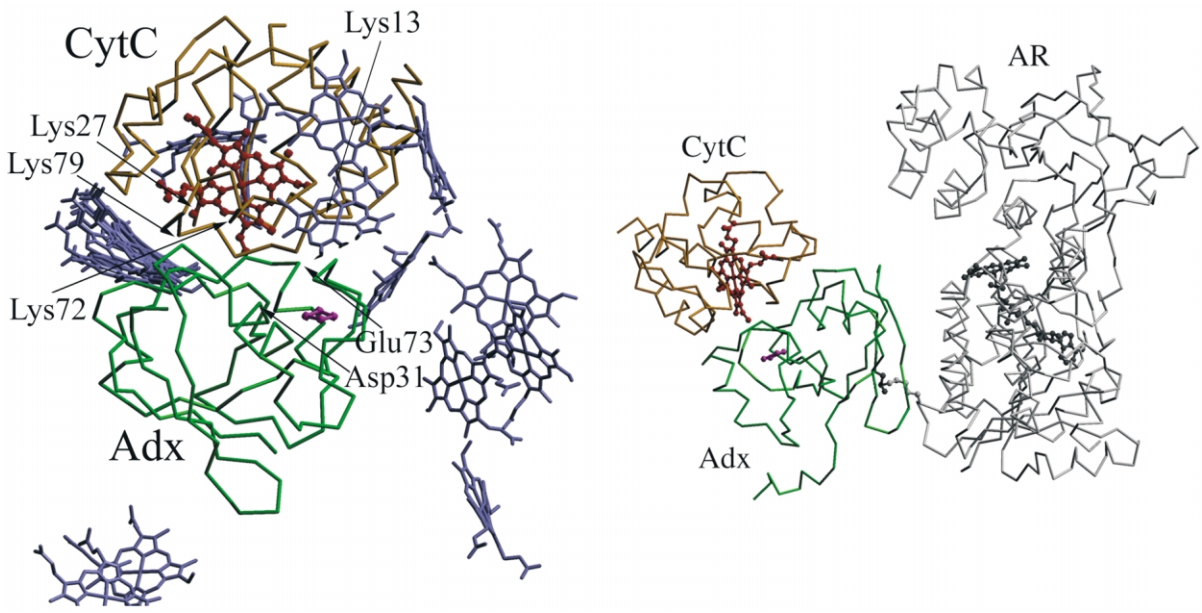

Fig. 6. Docking of Cyt*c* to Adx. (a) Minimum-energy configuration of an Adx–Cyt*c* complex formed by the free redox partners Adx (*green*) and Cyt*c* (*red–brown*). The 19 next-best Cyt*c* positions are marked by their hemes. (b) Putative configuration of the minimum-energy Adx–Cyt*c* complex in an electron transfer assay with the covalently cross-linked Adx–AR complex. The Adx (*green*) may freely rotate around the marked covalent cross-link. Figures were produced with SETOR [32].

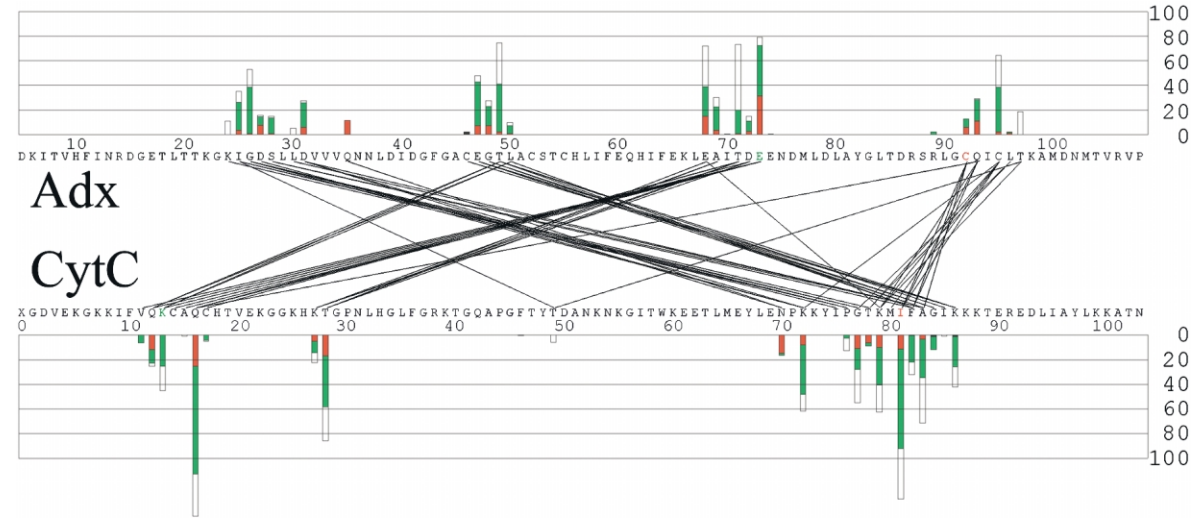

Fig. 7. Tentative interaction map for the model complex of Adx–Cyt*c*. The bars indicate the surface area per amino-acid side chain (Å^2) buried by contacts to amino acids of the other protein. Polar/polar contact areas are shown in red, hydrophobic/hydrophobic areas as open bars and mixed-type contact areas in green. The putatively cross-linked residues [34] are colored green, and residues colored red mark the likely electron pathway. This figure was produced with XSAE (C. Broger, personal communication).

are grateful to C. Jung (MDC) for critically reading the manuscript. We also thank U. Ryde, Lund (Sweden), for AMBER parameters of NADP. Supported by the Deutsche Forschungsgemeinschaft through He 1318/19 and WER436, and the Fonds der Chemischen Industrie.

References

[1] A. Müller, J.J. Müller, Y.A. Muller, H. Uhlmann, R. Bernhardt, U. Heinemann, New aspects of electron transfer revealed by the crystal structure of a truncated bovine adrenodoxin, Adx(4–108), Structure 6 (1998) 269–280.

[2] G.A. Ziegler, C. Vonrhein, I. Hanukoglu, G.E. Schulz, The structure of adrenodoxin reductase of mitochondrial P450 systems: electron transfer for steroid biosynthesis, J. Mol. Biol. 289 (1999) 981–990.

[3] G.A. Ziegler, G.E. Schulz, Crystal structures of adrenodoxin reductase in complex with $NADP^+$ and NADPH suggesting a mechanism for the electron transfer of an enzyme family, Biochemistry 39 (2000) 10986–10995.

[4] J.J. Müller, A. Lapko, G. Bourenkov, K. Ruckpaul, U. Heinemann, Adrenodoxin reductase–adrenodoxin complex structure suggests electron transfer path in steroid biosynthesis, J. Biol. Chem. 276 (2001) 2786–2789.

[5] L.M. Geren, F. Millett, Interaction between adrenodoxin and cytochrome *c*, J. Biol. Chem. 256 (1981) 4851–4855.

[6] Y. Sagara, T. Hara, Y. Ariyasu, A. Kajiyama, T. Yasukochi, T. Horiuchi, Different effects of carboxy-terminal deletion in the adrenodoxin molecule on cytochrome *c* and acetylated cytochrome *c* reductions, Biol. Pharm. Bull. 19 (1996) 1401–1406.

[7] V.M. Coghlan, L.E. Vickery, Site-specific mutations in human ferredoxin that affect binding to ferredoxin reductase and cytochrome P450scc, J. Biol. Chem. 266 (1991) 18606–18612.

[8] V.M. Coghlan, L.E. Vickery, Electrostatic interactions stabilizing ferredoxin electron transfer complexes. Disruption by 'conservative' mutations, J. Biol. Chem. 267 (1992) 8932–8935.

[9] M.E. Brandt, L.E. Vickery, Charge pair interactions stabilizing ferredoxin–ferredoxin reductase complexes. Identification by complementary site-specific mutations, J. Biol. Chem. 268 (1993) 17126–17130.

[10] T. Hara, T. Miyata, Identification of a cross-linked peptide of a covalent complex between adrenodoxin reductase and adrenodoxin, J. Biochem. 110 (1991) 261–266.

[11] A. Lapko, A. Müller, O. Heese, K. Ruckpaul, U. Heinemann, Preparation and crystallization of a cross-linked complex of bovine adrenodoxin and adrenodoxin reductase, Proteins: Struct. Funct. Genet. 28 (1997) 289–292.

[12] E.-C. Müller, A. Lapko, A. Otto, J.J. Müller, K. Ruckpaul, U. Heinemann, Covalently cross-linked complexes of bovine adrenodoxin with adrenodoxin reductase and cytochrome P450scc, Eur. J. Biochem. 268 (2001) 1837–1843.

[13] P.F. Churchill, L.R. deAlvare, T. Kimura, Topological studies of the steroid hydroxylase complexes in bovine adrenocortical mitochondria, J. Biol. Chem. 253 (1978) 4924–4929.

[14] L.M. Geren, F. Millett, Fluorescence energy transfer studies of the interaction between adrenodoxin and cytochrome *c*, J. Biol. Chem. 256 (1981) 10485–10489.

[15] T. Manabe, T. Kimura, A complex formation of the adrenal iron–sulfur protein (adrenodoxin) with cytochrome *c* and the decomposition of the iron–sulfur center, FEBS Lett. 47 (1974) 113–116.

[16] J.D. Lambeth, D.W. Seybert, J.R. Lancaster, J.C. Salerno, H. Kamin, Steroidogenic electron transport in adrenal cortex mitochondria, Mol. Cell. Biochem. 45 (1982) 13–31.

[17] T. Kido, T. Kimura, The formation of binary and ternary complexes of cytochrome P-450scc with adrenodoxin and adrenodoxin reductase–adrenodoxin complex. The implication in ACTH function, J. Biol. Chem. 254 (1979) 11806–11815.

[18] T. Hara, C. Koba, M. Takeshima, Y. Sagara, Evidence for the cluster model of mitochondrial steroid hydroxylase system derived from dissociation constants of the complex between adrenodoxin reductase and adrenodoxin, Biochem. Biophys. Res. Commun. 276 (2000) 210–215.

[19] G.W. Bushnell, G.V. Louie, G.D. Brayer, High-resolution three-dimensional structure of horse heart cytochrome *c*, J. Mol. Biol. 214 (1990) 585–595.

[20] H.M. Berman, J. Westbrook, Z. Feng, et al., The Protein Data Bank, Nucleic Acids Res. 28 (2000) 235–242.

[21] M.E. Davis, J.D. Madura, B.A. Luty, J.A. McCammon, Electrostatics and diffusion of molecules in solution: simulation with the University of Houston Brownian dynamics program, Comp. Phys. Commun. 62 (1991) 187–197.

[22] L.F. Ten Eyck, J. Mandell, V.A. Roberts, M.E. Pique, Surveying molecular interactions with DOT, in: A. Hayes, M. Simmons (Eds.), Proceedings of the 1995 ACM/IEEE Supercomputing Conference, IEEE Computer Society Press, Los Alamitos, CA, 1995, pp. 1–11.

[23] A.T. Brünger, P.D. Adams, G.M. Clore, et al., Crystallography & NMR system: a new software suite for macromolecular structure determination, Acta Crystallogr. D 54 (1998) 905–921.

[24] D.A. Pearlman, D.A. Case, J.W. Caldwell, et al., AMBER, a package of computer programs for applying molecular mechanics, normal mode analysis, molecular dynamics and free energy calculations to simulate the structural and energetic properties of molecules, Comp. Phys. Commun. 91 (1995) 1–41.

[25] V.A. Roberts, M.E. Pique, Definition of the interaction domain for cytochrome *c* on cytochrome *c* oxidase, J. Biol. Chem. 274 (1999) 38051–38060.

[26] H. Uhlmann, R. Kraft, R. Bernhardt, C-terminal region of adrenodoxin affects its structural integrity and determines differences in its electron transfer function to cytochrome P-450, J. Biol. Chem. 269 (1994) 22557–22564.

[27] L. Lo Conte, C. Chothia, J. Janin, The atomic structure of protein–protein recognition sites, J. Mol. Biol. 285 (1999) 2177–2198.

[28] D.N. Beratan, J.N. Betts, J.N. Onuchic, Protein electron transfer rates set by bridging secondary and tertiary structure, Science 252 (1991) 1285–1288.

[29] R. Morales, M.H. Charon, G. Kachalova, et al., A redox-dependent interaction between two electron-transfer partners involved in photosynthesis, EMBO Rep. 1 (2000) 271–276.

[30] G. Kurisu, M. Kusunoki, E. Katoh, et al., Structure of the electron transfer complex between ferredoxin and ferredoxin–$NADP^+$ reductase, Nat. Struct. Biol. 8 (2001) 117–121.

[31] H. Pelletier, J. Kraut, Crystal structure of a complex between electron transfer partners, cytochrome *c* peroxidase and cytochrome *c*, Science 258 (1992) 1748–1755.

[32] S.V. Evans, SETOR: hardware lighted three-dimensional solid model representations of macromolecules, J. Mol. Graph. 11 (1993) 134–138.

[33] R.E. Blankenship, It takes two to tango, Nat. Struct. Biol. 8 (2001) 94–95.

[34] L.M. Geren, P. O'Brien, J. Stonehuerner, F. Millett, Identification of specific carboxylate groups on adrenodoxin that are involved in the interaction with adrenodoxin reductase, J. Biol. Chem. 259 (1984) 2155–2160.

[35] S. Ferguson-Miller, D.L. Brautigan, E. Margoliash, Definition of cytochrome *c* binding domains by chemical modification. III. Kinetics of reaction of carboxydinitrophenyl cytochrome *c* with cytochrome *c* oxidase, J. Biol. Chem. 253 (1978) 149–159.

[36] J.D. Lambeth, L.M. Geren, F. Millett, Adrenodoxin interaction with adrenodoxin reductase and cytochrome P450scc, J. Biol. Chem. 259 (1984) 10025–10029.

[37] T. Hara, T. Kimura, Purification and catalytic properties of a cross-linked complex between adrenodoxin reductase and adrenodoxin, J. Biochem. 105 (1989) 594–600.

[38] J.J. Müller, A. Müller, M. Rottmann, R. Bernhardt, U. Heinemann, Vertebrate-type and plant-type ferredoxins: crystal structure comparison and electron transfer pathway modelling, J. Mol. Biol. 294 (1999) 501–513.

[39] J.D. Lambeth, H. Kamin, Adrenodoxin reductase–adrenodoxin complex. Flavin to iron–sulfur electron transfer as the rate-limiting step in the NADPH–cytochrome *c* reductase reaction, J. Biol. Chem. 254 (1979) 2766–2774.

[40] L.E. Vickery, Molecular recognition and electron transfer in mitochondrial steroid hydroxylase systems, Steroids 62 (1997) 124–127.

[41] I. Pikuleva, K. Tesh, M.R. Waterman, Y. Kim, The tertiary structure of full-length bovine adrenodoxin suggests functional dimers, Arch. Biochem. Biophys. 373 (2000) 44–55.